

Search for lightest neutralino- and stau-pair production in light gravitino scenarios with stau NLSP

Preliminary

DELPHI Collaboration

G. Wolf ¹, R. Alemany ², C. García ², F.R. Cavallo ³, F.L. Navarria ³

Abstract

Promptly decaying lightest neutralino and long-lived stau pair-production are searched for in the context of light gravitino scenarios. It is assumed that the $\tilde{\tau}_1$ is the NLSP and the lightest neutralino is the NNLSP. Data collected with the Delphi detector at centre-of-mass energies from 161 to 183 GeV are analysed. No evidence of the production of these particles is found. Hence, lower mass limits for both kinds of particles are set at 95% C.L.. In the case of gaugino-like neutralinos, a limit $m_{\tilde{\chi}_1^0} > 71.5 - 81 \text{ GeV}/c^2$ is obtained. In the search for long-lived stau, masses $m_{\tilde{\tau}_R} < 70. - 77.5 \text{ GeV}/c^2$ are excluded for gravitino masses from 10 to 150 eV/c^2 . Combining this search with the searches for stable heavy leptons and MSSM staus allows to set a limit of $m_{\tilde{\tau}_R} < 68.5 \text{ GeV}/c^2$ independently of the gravitino mass.

Paper submitted to the ICHEP'98 Conference
Vancouver, July 22-29

¹ CERN, CH-1211 Geneva 23, Switzerland

² IFIC, Avda. Dr. Molliner 50. Burjassot 46100, Valencia, Spain

³ INFN, Bologna, V. le Berti Pichat 6/2, I00126 Bologna, Italy



1 Introduction

In models including supersymmetry, it is often assumed that the messengers of supersymmetry breaking interact with gravitational strength and that the breaking scale in a hidden sector is of the order of 10^{11} GeV. An alternative possibility is that supersymmetry is broken at some low scale (between the Planck and the electroweak scale), and that the ordinary gauge interaction acts as the messenger of supersymmetry breaking [1, 2]. In local supersymmetry, the Goldstino becomes the longitudinal component of the gravitino (\tilde{G}). In this case, the gravitino is naturally the lightest supersymmetric particle (LSP) and the lightest Standard Model superpartner is the next to lightest supersymmetry particle (NLSP). Then, the NLSP is unstable and decays to its Standard Model (SM) partner plus a gravitino.

Since the gravitino couplings are suppressed compared to electroweak and strong interactions, decays to the gravitino are only relevant for the NLSP and therefore the production of pairs of supersymmetric particles at high energy colliders would generally take place through Standard Model couplings¹. The supersymmetric particles cascade to NLSPs, which eventually decay to their SM partners and a gravitino. The specific signatures of such decays depend crucially on the quantum numbers and composition of the NLSP, which are model dependent.

Although most of the attention has been focused on the case where the neutralino is the NLSP, it is equally possible that the NLSP is any other sparticle, and in particular a charged lepton. The number of $5 + \bar{5}$ generations of gauge mediating messengers, over most of the parameter space, determines what particle is the NLSP [3, 4, 5, 6]. For example, for one generation of $5 + \bar{5}$ the lightest neutralino tends to be the NLSP, while for two or more generations the balance tips towards right handed sleptons. Moreover, when left-right sfermion mixing is taken into account [7], the corresponding $\tilde{\tau}$ state, $\tilde{\tau}_1$, becomes the NLSP.

Throughout this work, it will be assumed that the $\tilde{\tau}_1$ is the NLSP, and that the lightest neutralino ($\tilde{\chi}_1^0$) is the *next-to*-NLSP (NNLSP). The $\tilde{\tau}_1$ width is given (independently of the $\tilde{\tau}$ mixing) by the two-body equation:

$$\Gamma(\tilde{\tau}_1 \rightarrow \tau + \tilde{G}) = \frac{m_{\tilde{\tau}_1}^5}{48\pi M_p^2 m_{\tilde{G}}^2} \quad (1)$$

where massless τ has been considered and M_p is the Planck mass. The mean decay length obtained from equation (1):

$$L = 1.76 \times 10^{-3} (E^2/m_{\tilde{\tau}_1}^2 - 1)^{\frac{1}{2}} \left(\frac{m_{\tilde{\tau}_1}}{100 \text{ GeV}/c^2} \right)^{-5} \left(\frac{m_{\tilde{G}}}{1 \text{ eV}/c} \right)^2 \text{ cm} \quad (2)$$

depends strongly on the $\tilde{\tau}_1$ mass and the gravitino mass ($m_{\tilde{G}}$). E is the energy of the $\tilde{\tau}_1$. The dependence of the mean decay length (L) on $m_{\tilde{G}}$ could be also interpreted in terms of the supersymmetry breaking scale (\sqrt{F}), through the relation:

$$m_{\tilde{G}} = \frac{F}{\sqrt{3}M_p} \simeq 2.5 \left(\frac{\sqrt{F}}{100 \text{ TeV}} \right)^2 \text{ eV}/c^2 \quad (3)$$

¹One exception to this rule being the process $e^+e^- \rightarrow Z^*/\gamma^* \rightarrow \tilde{G}\tilde{\chi}_1^0$, for the case of ultra-light \tilde{G} .

For \sqrt{F} between roughly 100-1000 TeV, the decay can take place within the detector. This range of \sqrt{F} is in fact consistent with astrophysical and cosmological considerations [8].

This note describes two searches: firstly $\tilde{\chi}_1^0$ -pair production, followed by the decay $\tilde{\chi}_1^0 \rightarrow \tilde{\tau}_1 \tau$. The $\tilde{\tau}_1$ decays promptly into $\tilde{\tau}_1 \rightarrow \tau \tilde{G}$. Thus, the signature of the signal would be four τ 's plus missing energy and momentum from the two gravitinos (plus the energy and momentum carried away by the neutrinos of the decay of the τ 's).

Secondly, the search for $\tilde{\tau}_1$ pair-production followed by the decays $\tilde{\tau}_1 \rightarrow \tau \tilde{G}$ within the detector volume, assuming conservatively the $\tilde{\tau}_1$ to be right-handed. The signature of such an event will be a track with a kink or a decay vertex when the $\tilde{\tau}_1$ decays inside the tracking devices. If the decay length is too short (small $m_{\tilde{G}}$) to allow the reconstruction of the $\tilde{\tau}_1$ track, only the decay products of the τ will be seen in the detector, and the search will then be based on track impact parameters. However, if the decay takes place outside the tracking devices (large $m_{\tilde{G}}$), the signature will be that of a heavy charged particle already studied in DELPHI [9]. For very light $m_{\tilde{G}}$ the limits from the search of MSSM stau can be applied [10]. All these searches have been combined to obtain a limit on $m_{\tilde{\tau}_R}$ independent on the \tilde{G} mass.

As it will be seen in section 4, together with the searches for $\tilde{\chi}_1^0 \rightarrow \gamma \tilde{G}$ [11] (in the $\tilde{\chi}_1^0$ NLSP scenario) and promptly decaying $\tilde{\tau}_1$ pair-production [10], these two searches complement each other for different domains of the gravitino mass.

The experimental procedure and event selection are described in section 2 and the results are presented in section 4.

2 Event sample and experimental procedure

The search for neutralino pair production is based on data collected by the DELPHI collaboration during 1996 and 1997 at centre of mass energies of 161, 172 and 183 GeV. The total integrated luminosities for the three centre of mass energies are 9.7, 10.4 and 53.9 pb^{-1} respectively. The search for stau pair production with big impact parameters and secondary vertices is based on data collected by the DELPHI collaboration during 1997 since the results obtained with the data collected in 1995 (at $\sqrt{s} = 130 - 136$ GeV) and 1996 are already published in [12]. The present analysis updates those results. The search for stau pair production with small impact parameters is based on data collected from 1995 to 1997. A detailed description of the DELPHI detector can be found in [13] and its performance in [14].

To evaluate the signal efficiencies and background contaminations, events were generated using different programs, all relying on JETSET 7.4 [15], tuned to LEP 1 data [16], in what concerns quark fragmentation. The program SUSYGEN [17] was used to generate the neutralino-pair events, and their subsequent decay products. In order to compute detection efficiencies, a total of 3000, 10000 and 14000 events with centre of mass energies of 161, 172 and 183 GeV respectively, and masses $45 \text{ GeV}/c^2 \leq m_{\tilde{\tau}_1} \leq m_{\tilde{\chi}_1^0} - 2 \text{ GeV}/c^2$, $m_{\tilde{\tau}_1} + 2 \text{ GeV}/c^2 \leq m_{\tilde{\chi}_1^0} < \sqrt{s}/2$. A stau pair sample of 18000 (subdivided in 15 samples) were produced with PYTHIA 5.7 [15] with mean decay lengths varied between 0.25 and 1000 cm, stau masses between 40 and 90 GeV/c^2 and 183 GeV centre of mass energy. Another sample of 35000 stau pairs was produced with SUSYGEN for the small impact parameter search (see below), with centre of mass energies ranging from 130 GeV up to

183 GeV.

The background process $e^+e^- \rightarrow q\bar{q}(n\gamma)$ was generated with PYTHIA 5.7, while DYMUS [18] and KORALZ [19] were used for $\mu^+\mu^-(\gamma)$ and $\tau^+\tau^-(\gamma)$, respectively. The generator of reference [20] was used for $e^+e^- \rightarrow e^+e^-$ events.

Processes leading to four-fermion final states, $(Z/\gamma)^*(Z/\gamma)^*$, W^+W^- , $W\nu_e$ and Ze^+e^- , were also generated using PYTHIA. The calculation of the four-fermion background was verified using the program EXCALIBUR [21], which consistently takes into account all amplitudes leading to a given four-fermion final state.

Two-photon interactions leading to hadronic final states were generated using TWOGAM [22], separating the VDM, QPM, and QCD components. The generators of Berends, Daverveldt and Kleiss [23] were used for the leptonic final states.

The cosmic background was studied using the cosmic data collected before the beginning of the 1997 LEP run.

The generated signal and background events were passed through the detailed simulation of the DELPHI detector and then processed with the same reconstruction and analysis programs used for real data.

3 Data selection

3.1 Neutralino pair production

In this section, the selection of the search for the process $e^+e^- \rightarrow \tilde{\chi}_1^0\tilde{\chi}_1^0 \rightarrow \tilde{\tau}_1\tau\tilde{\tau}_1\tau \rightarrow \tau\tilde{G}\tau\tilde{G}\tau$ is presented. The following cuts were applied in order to reduce the SM background preserving the signal efficiency:

The preselections of charged track and neutral cluster are described in ref. [24]. To assure good quality of the data, the ratio of good charged tracks to total number of tracks was required to be above 0.7. Charged tracks that do not pass quality cut selection but have an associated calorimetric energy of at least 2 GeV are recovered and their momentum is taken to be this associated energy. The events were to have at least 4 and at most 10 good charged tracks, where the recovered tracks are not counted as good tracks. In addition, in order not to process the bulk of the events of both data and background Monte Carlo samples, the thrust, the transverse momentum and the absolute value of the cosine of the θ angle of the missing momentum vector (θ_{miss}) were required to be smaller than 0.99, bigger than 3 GeV/c, and smaller than 0.95 respectively. Very forward-going events were eliminated by requiring that the energy in a cone of 30° around the beam-pipe be less than 70% of the total visible energy. With this preselection, the total Monte Carlo sample and data events were reduced by a factor of the order of 6000. Only the events passing the preselection were further analysed.

In order to optimise the cuts, it was noticed that signal events can be separated into two different kinematic regions of the $(m_{\tilde{\chi}_1^0}, m_{\tilde{\tau}_1})$ space: when the mass difference $\Delta_m = m_{\tilde{\chi}_1^0} - m_{\tilde{\tau}_1}$ is around or bigger than 10 GeV/c², all 4 τ 's carry similar momenta. When the difference becomes smaller, the two τ 's coming from the decay of the $\tilde{\tau}_1$ tend to be the most energetic, the more with increasing $\tilde{\chi}_1^0$ mass. The Durham algorithm [25] was used to divide the event in four jets by letting y_{cut} move as a free variable. Numbering

the jets from 1 to 4 with $E_1 > \dots > E_4$, we defined the following variable r :

$$r = \frac{E_3 + E_4}{E_1 + E_2} \quad (4)$$

An example of the distribution of r for two Δ_m can be seen in figure 1. It should be noticed that the distribution of r shifts towards lower values with increasing neutralino masses. The background Monte Carlo samples were then divided into two samples above and below $r = 0.1$ and cuts on a given variable were set to different values when necessary.

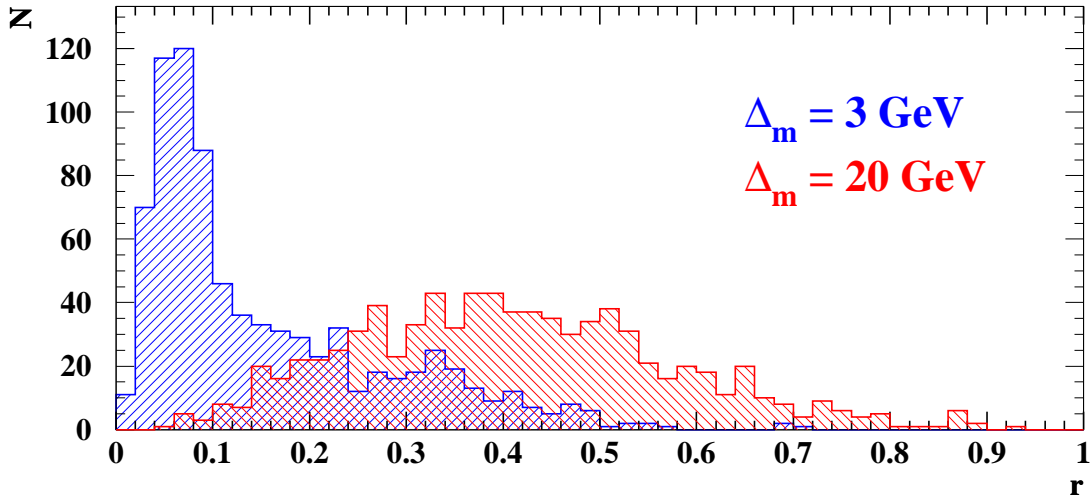


Figure 1: Distribution of the variable r . The positive slope hatched histogram shows r for $\Delta_m = 3 \text{ GeV}/c^2$. The negative slope hatched histogram shows r for $\Delta_m = 20 \text{ GeV}/c^2$.

Two sets of cuts were applied in order to reduce the $\gamma\gamma$ and $\bar{f}f(\gamma)$ backgrounds and a third set of cuts to select events according to their topology:

- 1- Cuts against $\gamma\gamma$ backgrounds: the transverse energy (E_T) should be bigger than 11 GeV for $r > .1$ ($E_T > 12 \text{ GeV}$ for $r \leq .1$). The energy in a cone of 30° around the beam axis was further restricted to be less than 60% of the total visible energy to avoid possible bias from the Monte Carlo samples. The missing mass should be smaller than $0.88\sqrt{s}$ ($0.9\sqrt{s}$). The momentum of the charged track with largest momentum (leading track) should be bigger than 4 GeV/c (3 GeV/c). After these cuts, the $\gamma\gamma$ background is reduced by a factor of the order of 30.
- 2- Cuts against $\bar{f}f(\gamma)$ backgrounds: the number of good charged tracks should be smaller than 7 (9). The cut on thrust was further reduced from 0.99 to 0.975. Dividing each event into two jets with the Durham algorithm, its acoplanarity should be bigger than 8° . The missing mass of the events should be bigger than $0.3\sqrt{s}$. After these cuts, the $\bar{f}f(\gamma)$ background was reduced by a factor of the order of 15.

- 3- Cuts based on topology: signal events tend naturally to cluster into a 4-jet topology. All jets should be at least 17° away from the beam-pipe direction. When reduced by the jet algorithm into a 2-jet configuration, each of these jets should be broader than 20° . Finally, each jet should be separated from the others at least by 8° (4°).

As an example, figures 2 to 4 show the distributions corresponding to these selection cuts at $\sqrt{s} = 183$ GeV. Table 1 shows the evolution of the data, expected background and one of the signal samples throughout these cuts for the same centre of mass energy.

Cut	$\gamma\gamma$	$ff\gamma$	4-fermion	Total MC	Data	Signal
pre-selection	496 ± 16	44.5 ± 1.5	13.1 ± 0.6	554 ± 16	567	61.4%
1	18 ± 2	40.6 ± 1.4	12.1 ± 0.6	70.8 ± 2.6	84	59.2%
2	2.2 ± 0.6	2.9 ± 0.4	4.5 ± 0.4	9.6 ± 0.8	12	45.4%
3	0	0.23 ± 0.09	0.27 ± 0.07	0.50 ± 0.11	2	38.3%

Table 1: Evolution of data and Monte Carlo samples through the different cuts described in the text, at $\sqrt{s} = 183$ GeV. Signal corresponds to $m_{\tilde{\chi}_1^0} = 75$ GeV/ c^2 and $m_{\tilde{\tau}_1} = 55$ GeV/ c^2 .

After these cuts, an efficiency between 25 and 45% was obtained for the signal events, and an estimated background of 0.12 ± 0.08 , 0.15 ± 0.09 and 0.50 ± 0.11 at $\sqrt{s} = 161$, 172 and 183 GeV respectively.

3.2 Stau pair production

This section describes the selection criteria in the search for the process $e^+e^- \rightarrow \tilde{\tau}_1\tilde{\tau}_1 \rightarrow \tau\tilde{G}\tau\tilde{G}$. As described in section 1, the mean life-time of the $\tilde{\tau}_1$ depends of the mass of the gravitino. Thus, for a gravitino with a mass of the order of a few hundred eV/ c^2 or more, the stau would behave as stable for detection purposes. When the mass of the gravitino is between a few eV/ c^2 and a few hundred eV/ c^2 , one or both staus would decay in flight in some part of the detector, creating a well defined secondary vertex. This is described in subsection 3.2.1. If the mass of the gravitino is even smaller, stau pair production would produce displaced vertices. This is described in subsections 3.2.2 and 3.2.3.

3.2.1 Search for secondary vertices

This analysis exploits a peculiarity of the $\tilde{\tau}_1 \rightarrow \tau\tilde{G}$ topology in the case of intermediate mass gravitinos, namely, one or two tracks coming from the interaction point and at least one of them with either a secondary vertex or a kink. Reconstruction of secondary vertices is illustrated in figure 5, which shows a zoom of a decay vertex and the variables used in the analysis.

A rather loose set of general requirements was imposed on the events in order to suppress the low energy background (beam-gas, beam-wall, etc), $\gamma\gamma$, e^+e^- and hadronic events:

- charged multiplicity between 1 and 10,

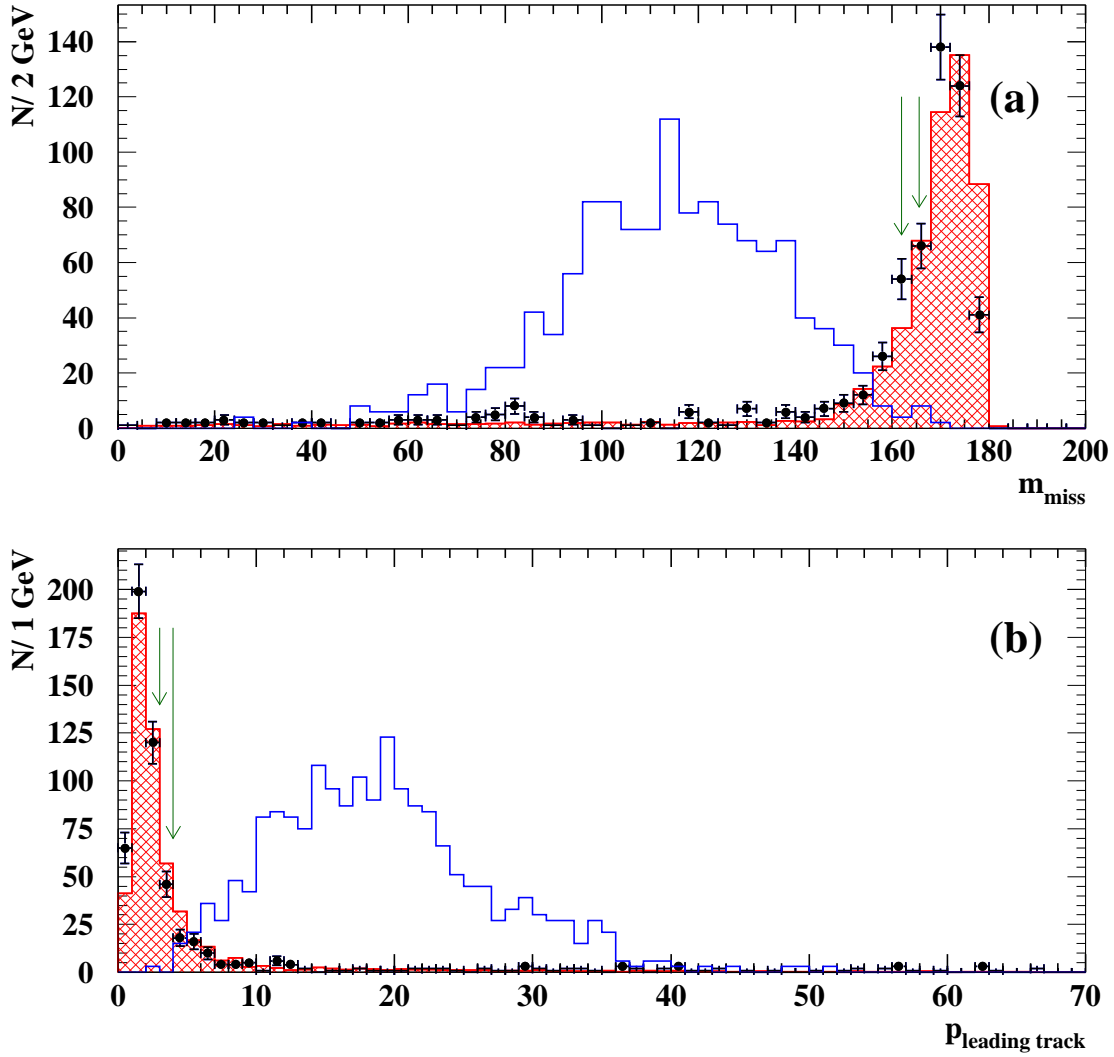


Figure 2: Missing Mass (a) and Momentum of the leading track (b) for data (dots), Standard Model Monte Carlo (crossed histogram) and one of the simulated signals with cross section not to scale (continuous line histogram) after preselection. Cuts for these variables are explained in the text and are shown with arrows.

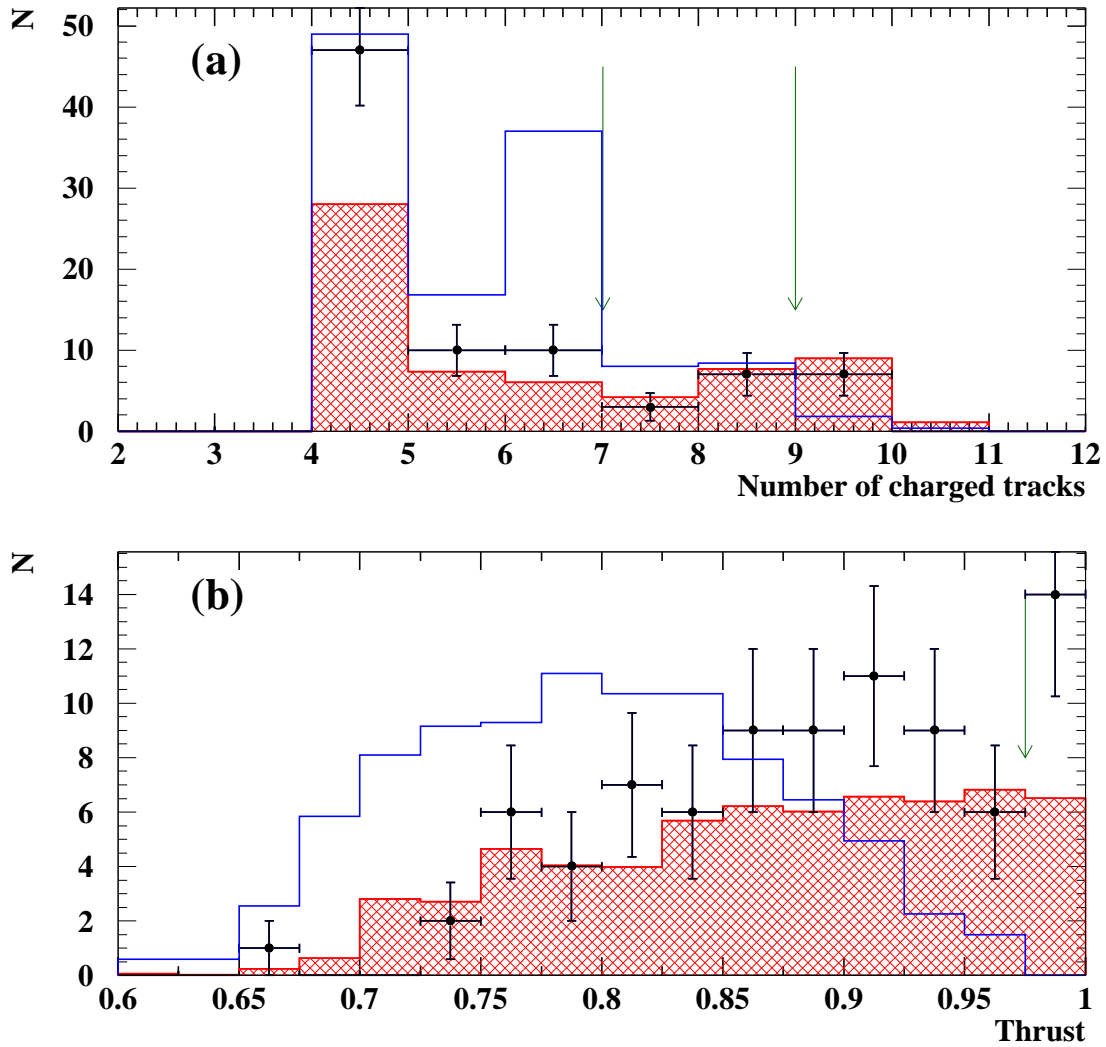


Figure 3: Number of charged tracks (a) and Thrust (b) for data (dots), Standard Model Monte Carlo (crossed histogram) and one of the simulated signals with cross section not to scale (continuous line histogram), after the cut to remove $\gamma\gamma$ events. Cuts for these variables are explained in the text and are shown with arrows.

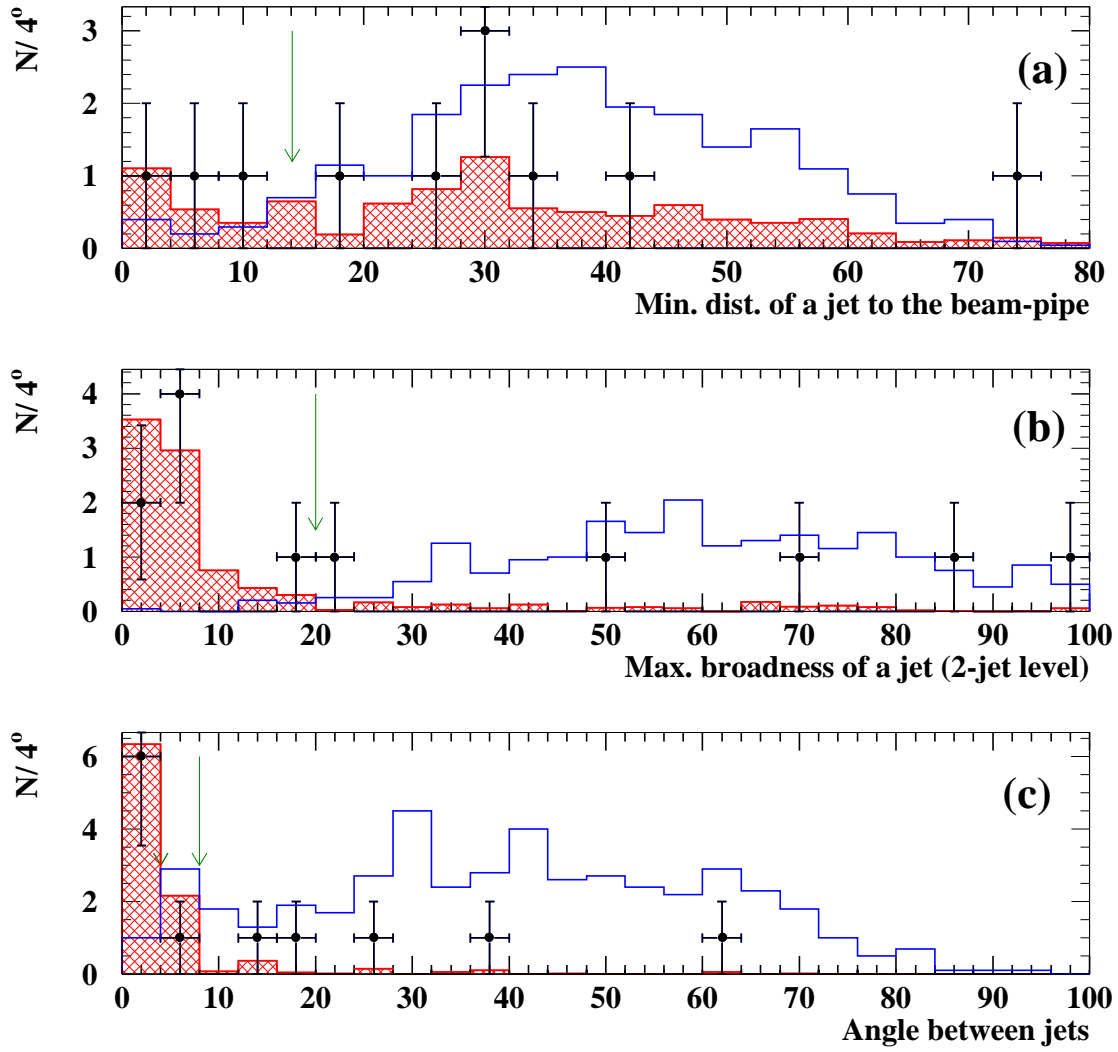


Figure 4: Minimum angular distance of a jet to the beam-pipe (a), Maximum angular broadness of a jet at the 2-jet level (b) and Angle between jets (c) for data (dots), Standard Model Monte Carlo (crossed histogram) and one of the simulated signals with cross section not to scale (continuous line histogram), after the cut to remove $f\bar{f}(\gamma)$ events. Cuts for these variables are explained in the text and are shown with arrows.

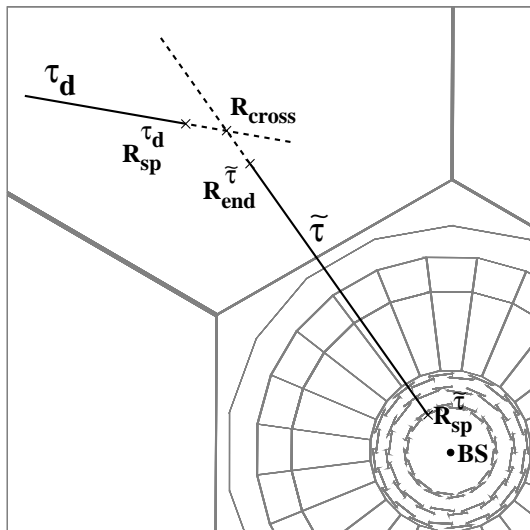


Figure 5: Sketch of a decay vertex that illustrates the reconstruction of a secondary vertex, shown in the plane perpendicular to the beam. The stau track (labelled with $\tilde{\tau}$) and the track of the decay product of the tau (labelled with τ_d) are extrapolated (dotted line). The extrapolated tracks define a crossing point (R_{cross}). $R_{sp}^{\tilde{\tau}}$ and $R_{end}^{\tilde{\tau}}$ are the first and last measured points of the $\tilde{\tau}$ track. $R_{sp}^{\tau_d}$ is the first measured point of track selected as the τ decay product. All the distances are measured with respect to the beam spot (BS).

- visible energy above 10 GeV,
- total electromagnetic energy below 40 GeV
- transverse momentum with respect to the beam axis (p_T) greater than 5 GeV/ c ,
- energy measured in the very forward calorimeters below 10 GeV,

leaving only about 0.6% of the whole data sample. To compute the above quantities the reconstructed charged particles were required to have momentum above 100 MeV/ c and impact parameter below 4 cm in the transverse plane and below 10 cm in the longitudinal direction. Clusters in the calorimeters were interpreted as neutral particles if they were not associated to charged particles and if their energy exceeded 100 MeV. However, no quality requirements were imposed on the reconstructed tracks in the following stages. All the charged tracks were grouped in clusters according to their first measured point (starting point). This clustering procedure is described in [26]. Each cluster contained all tracks whose starting points differ by less than 2 cm. The starting point of a cluster was defined as the average of the starting points of its tracks. This procedure allowed for clusters with a single track if its momentum was larger than 1.5 GeV/ c . Events were rejected if more than 6 tracks were not grouped in clusters or no cluster was found.

A cluster with only one track was considered a $\tilde{\tau}_1$ candidate track if:

- the distance of the first measured point to the beam spot in the plane transverse to the beam axis (xy plane), $R_{sp}^{\tilde{\tau}}$, was smaller than 10 cm,
- its momentum was greater than 2 GeV/ c ,
- $|\cos\theta| < 0.8$, where θ is the polar angle with respect to the beam axis,

- the impact parameter of the track along the beam axis and in the plane perpendicular to it were less than 10 and 4 cm, respectively.

For each $\tilde{\tau}_1$ candidate (single track cluster fulfilling the above conditions), a search was made for a second cluster with starting point in the transverse plane (xy plane) greater than $R_{\tilde{\tau}}^{sp}$, and an angular separation between the directions defined by the beam spot and the cluster starting points smaller than 90° in the xy plane. This second cluster was assumed to be formed by the decay products of the τ coming from the $\tilde{\tau}_1 \rightarrow \tau \tilde{G}$ process. Therefore, the $\tilde{\tau}_1$ candidate and the τ cluster had to define a secondary vertex. If the τ cluster included more than one track, only the track with the highest momentum was used to search for the decay vertex or kink (crossing point with the $\tilde{\tau}_1$ track).

The tracks were parametrised with respect to their perigee [27] to calculate the point of closest approach between both tracks (the candidate $\tilde{\tau}_1$ track and the selected track from the candidate τ cluster). The following conditions were required to define a good crossing point:

- the minimum distance between the tracks had to be smaller than 1 mm in the xy plane,
- the crossing point, the end point of the stau track and the starting point of the tau decay products were required to satisfy the following conditions:

$$\begin{aligned} -10 \text{ cm} &< (R_{cross} - R_{end}^{\tilde{\tau}}) < 25 \text{ cm} \\ -25 \text{ cm} &< (R_{cross} - R_{sp}^{\tau}) < 10 \text{ cm} \end{aligned}$$

where $R_{end}^{\tilde{\tau}}$, R_{cross} and R_{sp}^{τ} are the distance from the beam spot of the end point of the $\tilde{\tau}_1$ track, the crossing point of the tracks and the starting point of the τ decay track, in the xy plane. Figure 6 shows the distribution of these parameters.

Fake secondary vertices could be produced by particles interacting in the detector material or by radiated photons if the particle trajectory was reconstructed in two separate track. To eliminate this kind of events, additional requirements were imposed:

- to reject hadronic interactions in the detector walls, any hadronic interaction should be outside a 5° semi-cone w.r.t. the kink direction
- to reject photon radiation, in the case of τ clusters with only one track, no neutral particle had to be present in a 3° cone around the direction defined by the difference between the $\tilde{\tau}_1$ momentum and the momentum of the τ daughter,
- to reject segmented tracks, the angle between the momenta of the tracks used to define a vertex, calculated at the crossing point, had to be larger than 6° .

If no pair of tracks was found to fulfil these conditions, the event was rejected. Figure 7 shows the distribution of these three angles for real data, expected Standard Model background and simulated signal for 60 GeV/ c^2 $\tilde{\tau}_1$ decaying with a mean distance of 50 cm.

One event in real data was found to satisfy all the conditions described above. The event was inspected graphically and found to be a superposition of a low energy event with a cosmic muon crossing the detector, therefore it will not be considered as a candidate.

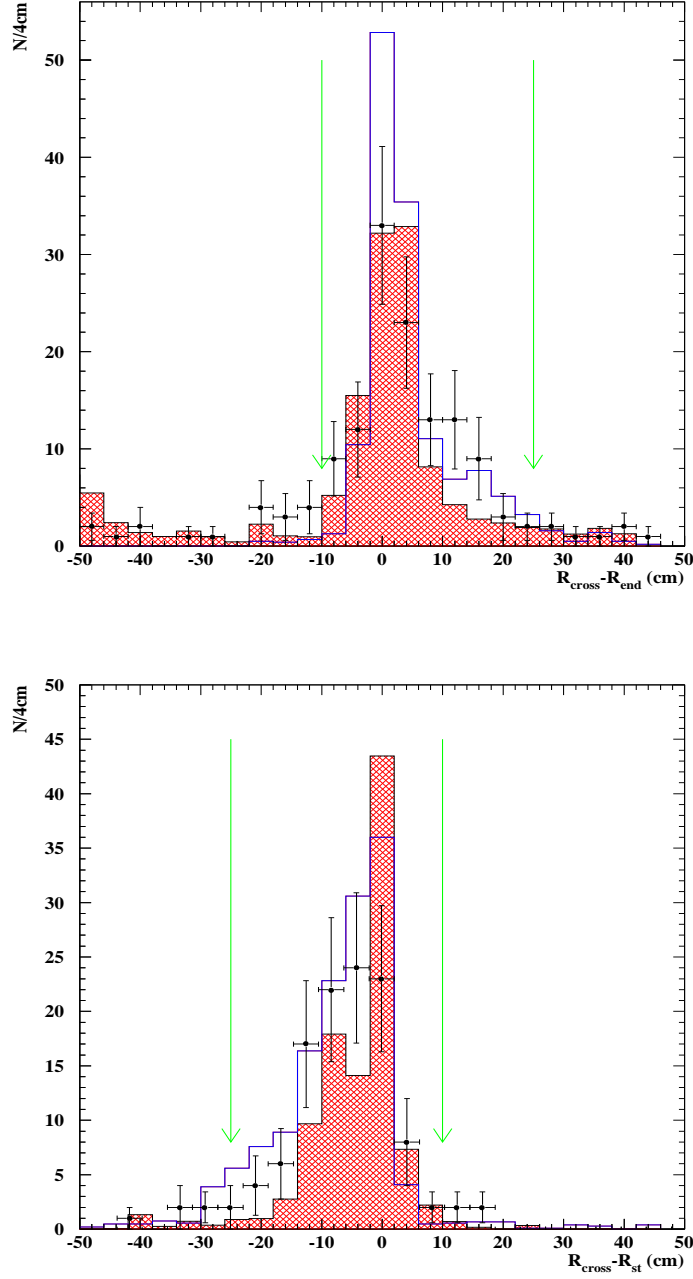


Figure 6: $R_{cross} - R_{end}^{\tilde{\tau}}$ and $R_{cross} - R_{sp}^{\tau}$ for real data (dots), expected Standard Model background (dark histogram) and simulated signal for $60 \text{ GeV}/c^2$ $\tilde{\tau}_1$ decaying with a mean distance of 50 cm (continuous line histogram). Cuts for these variables are explained in the text and are shown with arrows.

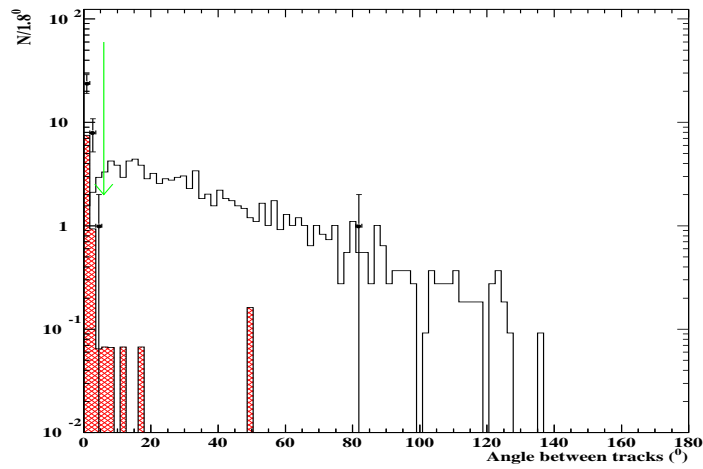
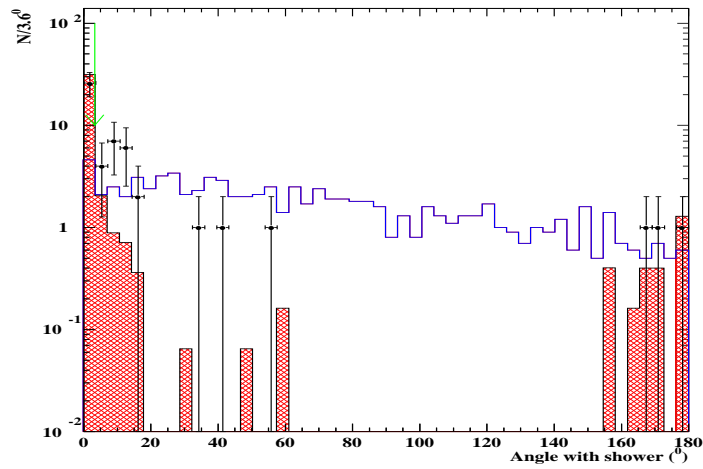
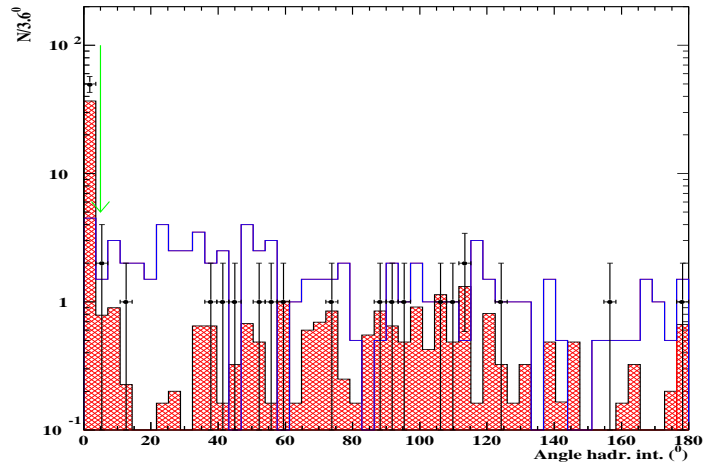


Figure 7: Angle between the hadronic interaction and the reconstructed kink (top plot), angle with the electromagnetic shower (middle plot) and angle between the tracks of the kink (bottom plot), for real data (dots), expected Standard Model background (dark histogram) and simulated signal for $60 \text{ GeV}/c^2 \tilde{\tau}_1$ decaying with a mean distance of 50 cm (continuous line histogram). Cuts for these variables are explained in the text and are shown with arrows.

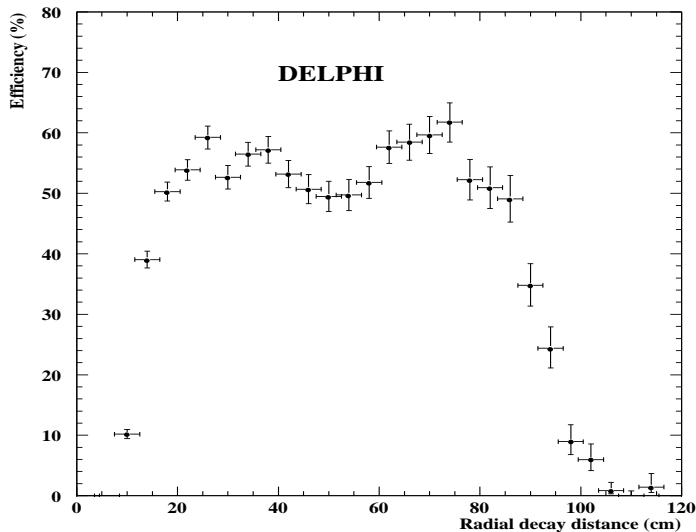


Figure 8: Efficiency of the vertex search versus the mean decay distance on the xy plane for a $\tilde{\tau}_1$ of $60 \text{ GeV}/c^2$ at a centre of mass energy of 183 GeV .

The vertex reconstruction was sensitive to decay lengths in the xy plane (R) (see figure 8) between 15 cm and 90 cm . Inside this region a vertex was reconstructed with an efficiency of $\sim 54\%$ since the VD (Vertex Detector) and the ID (Inner Detector) were needed to reconstruct the $\tilde{\tau}_1$ track and the TPC (Time Projection Chamber) to reconstruct the decay products. The efficiency dropped to zero for $\tilde{\tau}_1$ s decaying near the external edge of the TPC. The maximum efficiency ($\sim 79\%$) was reached when the two staus decay inside this sensitive region. The shape of the efficiency distribution remained the same, independently of the $\tilde{\tau}_1$ mass; it simply scaled down near the kinematic limit. The loss of efficiency near the kinematic limit is due to the fact that the $\tilde{\tau}_1$ boost is smaller and the kink reconstruction less efficient when the angles between the $\tilde{\tau}_1$ and the τ products increase.

The efficiencies for different mean decay lengths and $\tilde{\tau}_1$ masses were calculated by applying the above selections to the simulated signal samples. Figure 9 shows the efficiencies (ε_2) obtained for a $60 \text{ GeV}/c^2$ $\tilde{\tau}_1$ at a centre of mass energy of 183 GeV and for decay lengths from 0.25 to 1000 cm . For a mean decay length of 50 cm the vertex search efficiency is of the order of 55% .

3.2.2 Large impact parameter search

To investigate the region of low gravitino masses (short decay lengths) the previous search was extended to the case of the $\tilde{\tau}_1$ decaying between 0.25 cm and around 10 cm . In this case the $\tilde{\tau}_1$ track was not reconstructed in the ID and only the τ decay products were detected. The signature for this topology was tracks with large impact parameters and large acollinearities. Cosmic rays, badly reconstructed tracks or interactions in the detector material could result in large impact parameters. However, the two tracks in a cosmic event usually had impact parameters of the same order and opposite sign. The acollinear-

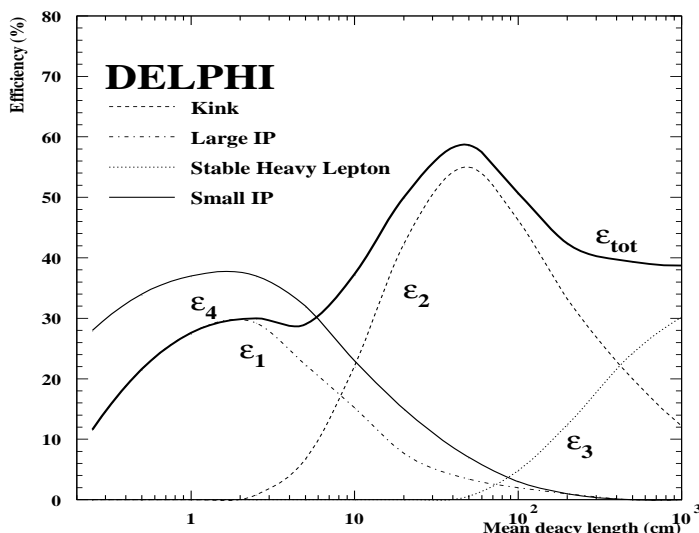


Figure 9: Efficiency of the big impact parameter search (ε_1), vertex search (ε_2), heavy lepton search (ε_3) [9] and combined efficiency (ε_{tot}) of these three searches. ε_4 corresponds to the large impact parameter search. These efficiencies have been calculated for a $\tilde{\tau}_1$ of $60 \text{ GeV}/c^2$ at a centre of mass energy of 183 GeV .

ity in events with badly reconstructed tracks or interactions was always small. Figures 10 and 11 show the two dimensional plot of the impact parameter and the acollinearity of two TPC track events for simulated signal of $60 \text{ GeV}/c^2$ $\tilde{\tau}_1$ with mean decay length of 2.5 cm , cosmic muons, Standard Model expected background and real data.

The impact parameter search was only applied to those events accepted by the general cuts, previously described, and not selected by the vertex analysis. The events were accepted as candidates if:

- there were two single track clusters in the event (i.e. two tracks with momentum larger than $1.5 \text{ GeV}/c$ and a distance between starting points larger than 2 cm),
- the first measured point of at least one of the tracks had to be within 12 cm of the beam axis,
- both tracks were reconstructed in the TPC to guarantee a good track reconstruction quality,
- at least one of the tracks had an impact parameter larger than 0.2 cm in the plane transverse to the beam axis, to remove standard events,
- the ratio of the impact parameters of the two tracks was smaller than -1.5 and larger than -0.5 , to reject cosmic rays,
- the acollinearity between the two tracks was larger than 10° ,
- the angle defined by the directions of the starting points of the tracks with respect to the the beam-spot was larger than 3° .

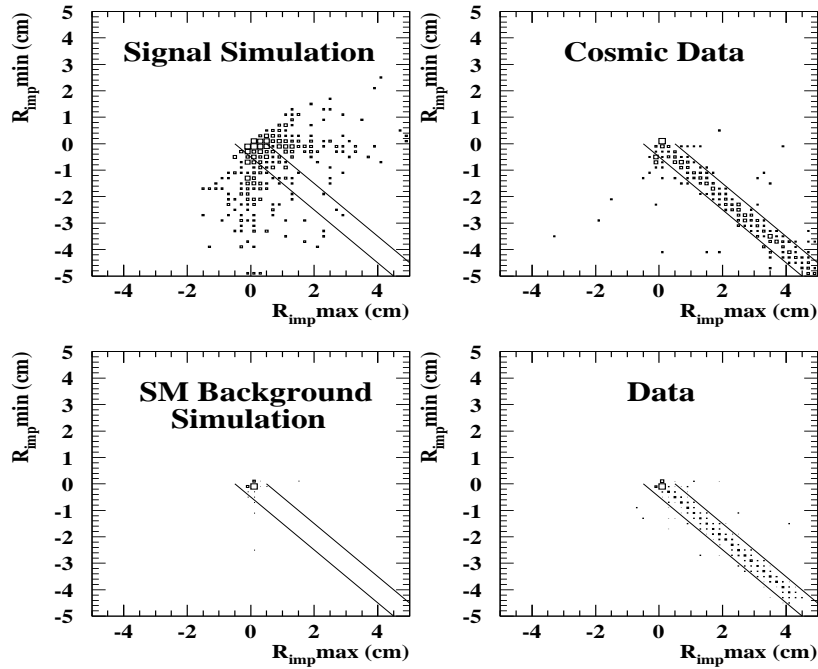


Figure 10: Impact parameters of two track events for simulated signal of $60 \text{ GeV}/c^2 \tilde{\tau}_1$ with mean decay length of 2.5 cm, cosmic muons, Standard Model expected background and real data.

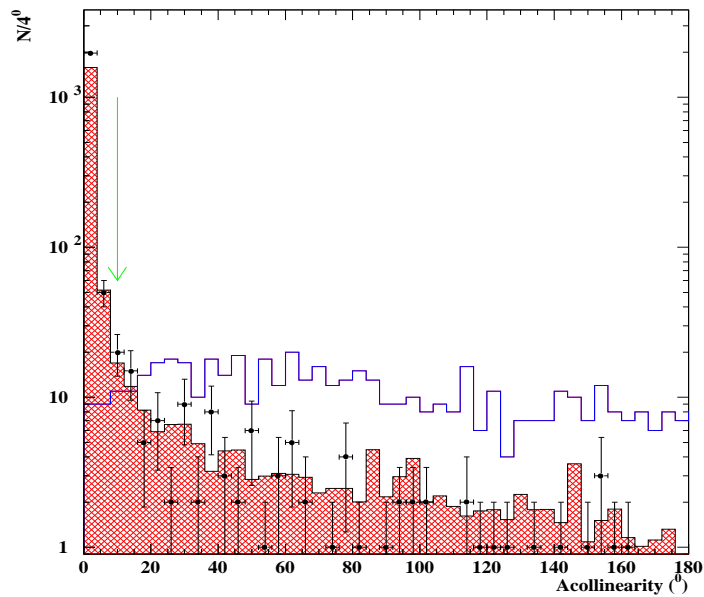


Figure 11: Acollinearity for real data (dots), expected Standard Model background (dark histogram) and simulated signal for $60 \text{ GeV}/c^2 \tilde{\tau}_1$ decaying with a mean distance of 50 cm (continuous line histogram). The cut for this variable is explained in the text and is shown with an arrow.

The efficiencies were derived for the different $\tilde{\tau}_1$ masses and decay lengths by applying the same selection to the simulated signal events. Figure 9 shows the efficiency of the large impact parameter search (ε_1) for a 60 GeV/ c^2 $\tilde{\tau}_1$ at a centre of mass energy of 183 GeV. The maximum efficiency was 29.2%, corresponding to a mean decay length of 2.5 cm, decreasing very fast for lower decay lengths due to the cut on minimum impact parameter. For longer decay lengths the efficiency decreased smoothly due to the cut on the maximum number of tracks because in this situation the $\tilde{\tau}_1$ track could be reconstructed. No dependence on the $\tilde{\tau}_1$ mass was found far from the kinematic limit. The losses of efficiency for $\tilde{\tau}$ masses near the kinematic limit and due to initial state radiation were also considered.

Trigger efficiencies were studied, simulating the DELPHI trigger response to the events selected by the vertex search and by the large impact parameter analysis, and were found to be around 99%.

No events in the real data sample were selected with the above criteria. The number of expected background events is shown in Table 2 for the combination of the vertex and large impact parameter searches.

Channel:	$\tilde{\tau}_1 \rightarrow \tau \tilde{G}$
Observed events	0
Total background	$0.63^{+0.55}_{-0.12}$
$Z^*/\gamma \rightarrow (\tau\tau)(n\gamma)$	$0.07^{+0.16}_{-0.06}$
$Z^*/\gamma \rightarrow (ee)(n\gamma)$	$0.09^{+0.19}_{-0.03}$
4-fermion (except $\gamma\gamma$)	$0.10^{+0.12}_{-0.06}$
$\gamma\gamma \rightarrow \tau^+\tau^-$	$0.20^{+0.27}_{-0.06}$
$\gamma\gamma \rightarrow e^+e^-$	$0.17^{+0.39}_{-0.05}$

Table 2: The number of observed events, together with the total number of expected background events and the expected numbers from the individual background sources, for both large impact parameter and secondary vertex searches combined.

3.2.3 Small Impact Parameter search

The previous search can be further extended down to mean decay lengths of around 0.1 cm. As already mentioned, cosmic radiation is a source of background to this search. For this reason, a loose impact parameter cut (≤ 10 cm in the xy plane, ≤ 15 cm along z), was applied besides other standard track quality selections based on momentum (≥ 400 MeV/ c), momentum error (≤ 100 %), polar angle ($\geq 20^\circ$) and track length (≥ 30 cm). All the neutrals ≥ 100 MeV were accepted. Any calorimetric deposit associated to a discarded charged track was regarded as a neutral track.

If the mean $\tilde{\tau}_1$ decay length was shorter than about 10 cm, the main sources of background were given by $\gamma\gamma$, γ^*/Z^* , Bhabha, eeZ^0 and Compton events. W pair

production contributed to the background, especially in the channel $WW \rightarrow \tau\nu\tau\nu$, which had a topology similar to the signal searched for and could only be reduced by a cut on the impact parameters.

This search was restricted to events with low charged multiplicity ($2 \leq N_{ch} \leq 4$) and large missing energy ($E_{mis} \geq 0.3 \sqrt{s}$). The $\gamma\gamma$ events were suppressed by a lower cut on the visible energy ($E_{vis} \geq 0.08 \sqrt{s}$) and transverse missing momentum ($P_T \geq 0.03 \sqrt{s}$); moreover the missing momentum direction was required to be in the barrel region ($30^\circ \leq \theta_{P_{miss}} \leq 150^\circ$) and the total energy in the forward and backward regions (30° around the beam direction) should not exceed 10% of the total visible energy in the event.

Standard $e^+e^- \rightarrow f\bar{f}(\gamma)$ processes and cosmics were reduced requiring the acollinearity to be $\geq 10^\circ$.

The event thrust direction was determined using the selected tracks, the event was then divided in two hemispheres by the plane normal to the thrust axis and the most energetic track in each hemisphere was found. These tracks are named in the following "leading tracks" (l.t.1, l.t.2). Further track quality requirements were only applied to the l.t.'s: each l.t. should not start at a distance larger than 50 cm from the beam spot in the xy plane, should have at least one track segment beyond the ID, and be out of the HPC cracks. In addition, at least one l.t. should have a track segment in the TPC.

A further reduction of the standard $e^+e^- \rightarrow f\bar{f}(\gamma)$ and cosmic backgrounds was obtained by requiring that the angle between the l.t.'s in the xy plane was less than 3 radians. Other cuts were used to reject hadronic events ($\sqrt{p_{l.t.1}^2 + p_{l.t.2}^2} \geq 0.03\sqrt{s}$), Bhabha events ($E_{e.m.}(l.t.1) + E_{e.m.}(l.t.2) \leq 0.35E_{CM}$), residual cosmics (any l.t. with an impact parameter larger than 1 cm in the xy plane, should be reconstructed in the TPC and at least another detector) and γ conversions (if there were only 2 charged tracks in the event, they should form an angle greater than 1°).

The background left after the application of the selection described above is mainly due to events containing τ pairs in the final state: namely $\gamma^*/Z^* \rightarrow \tau\tau$ and $WW \rightarrow \tau\nu\tau\nu$. To reject these events, the variable $IP_c = \sqrt{i.p.^2_{l.t.1} + i.p.^2_{l.t.2}}$ was used, where the i.p. are the impact parameters defined in the xy plane. The IP_c distribution for the simulated signal and $\gamma^*/Z^* \rightarrow \tau\tau$ events, without any preselection, is shown as an example in figure 12. Figure 13 shows the IP_c distribution of the selected real data and the total residual simulated background. A cut $IP_c \geq 600\mu m$ was therefore chosen to reject most of the remaining background.

Applying these cuts to the simulated signal events, the efficiency turned out not to depend separately on the centre of mass energy and on the $\tilde{\tau}_1$ mass but rather on the $\tilde{\tau}_1$ decay length in the laboratory system, which is determined by both these variables. Figure 9 shows the efficiency (ε_4) of the small impact parameter search as a function of the $\tilde{\tau}_1$ decay length. The cut on IP_c is the cause of the drop in efficiency at small decay lengths, whilst at large decay lengths the loss of efficiency is due to the upper impact parameter cut used in the track selection.

The non negligible background contributions normalized to the integrated luminosities of the four samples, are shown in table 3, together with the selected data events. As expected, the main sources of background come from channels containing τ 's in the final state.

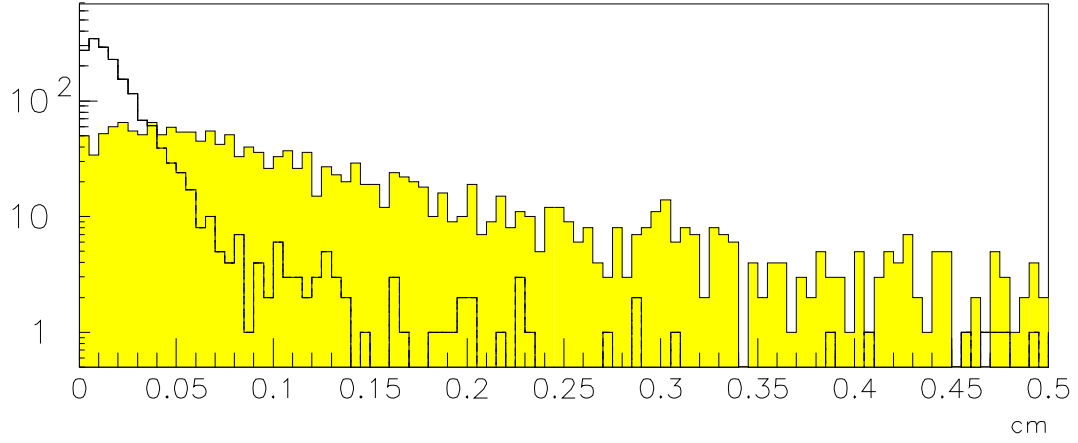


Figure 12: IP_c distribution for standard $\gamma Z^0 \rightarrow \tau\tau$ events and for $\tilde{\tau}_1\tilde{\tau}_1$ events (shaded) with a mean decay length of 2.1 mm.

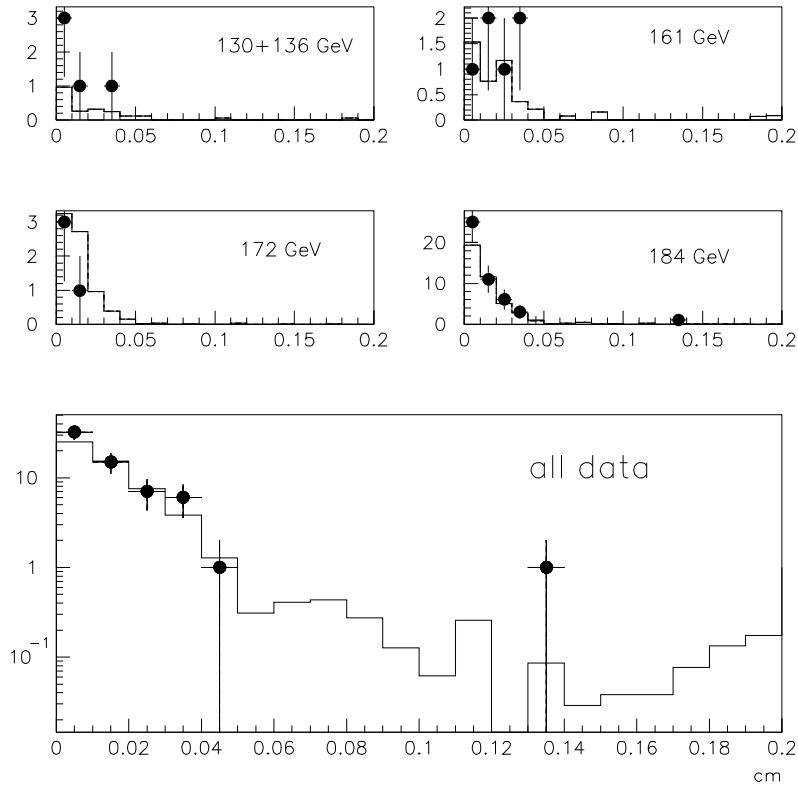


Figure 13: IP_c distribution for the total Standard Model background (solid) and the selected real events (dots).

channel	130 GeV+ 136 GeV	161 GeV	172 GeV	183 GeV
$\gamma\gamma \rightarrow \tau\tau$	$0_{-0}^{+0.65}$	0.09 ± 0.09	$0_{-0}^{+0.08}$	0.20 ± 0.20
$\gamma^*/Z^* \rightarrow \tau\tau$	0.19 ± 0.11	0.21 ± 0.12	0.07 ± 0.05	1.00 ± 0.26
WW	-	0.03 ± 0.01	0.12 ± 0.04	0.77 ± 0.12
ZZ	-	-	-	0.02 ± 0.02
$ee\tau\tau$	10^{-3}	0.16 ± 0.16	$0_{-0}^{+0.05}$	10^{-3}
total	$0.19_{-0.11}^{+0.66}$	0.48 ± 0.22	$0.20_{-0.06}^{+0.11}$	2.0 ± 0.35
candidates	0	0	0	1

Table 3: Expected background events (Monte Carlo) and selected data events at the various centre of mass energies.

4 Results and interpretation

4.1 Neutralino pair production


No data event passes the cuts at $\sqrt{s} = 161$ or 172 GeV. Two data events were observed to pass all the cuts at $\sqrt{s} = 183$ GeV. They are shown in figures 14 and 15.

Their main features are listed in Table 4. Both of them can be interpreted as being 4-fermion events. The first event has an electron, a low energy particle that could either be a muon or a pion, a pion and a very soft particle that could possibly be identified as a pion or a muon. The event could be described as $\gamma^*\gamma^*$, each virtual photon going into a pair of τ s. The second event contains a muon, two energetic electrons and a pion. It could be described as a $Z^*\gamma^*$ event, with $Z^* \rightarrow e^+e^-$, and $\gamma^* \rightarrow \tau^+\tau^-$.

	Candidate 1	Candidate 2
r	.14	.31
p_T	8.7	9.2
m_{miss}	139.5	63.8
thrust	0.91	0.84
E_{30}/E_{vis}	0.45	0.62
E_{TR}	28.	78.6
acoplanarity	8.6°	15.9°
Num. of charged tracks	4	6
Min. angle between jets	63°	$26.^\circ$
P of track with max momentum	17.8	43.7

Table 4: Some characteristics of the two candidates found at $\sqrt{s} = 183$ GeV.

Since no evidence for a signal was found in the data, a limit on the production cross

 DELPHI Beam: 91.6 GeV DAS: 14-Sep-1997 18:45:01	Run: 77798	Evt: 3574								
	Proc: 2-Dec-1997									
	Scan: 5-Mar-1998									
	Tan+DST									
				TD	TE	TS	TK	TV	ST	PA
Act	0	39	0	4	0	0	0	0	0	0
	(87	X 98	I	0	I	4	I	0	I	0
Deact	0	0	0	0	0	0	0	0	0	0
	(0	X	0	X	0	X	9	I	0	I

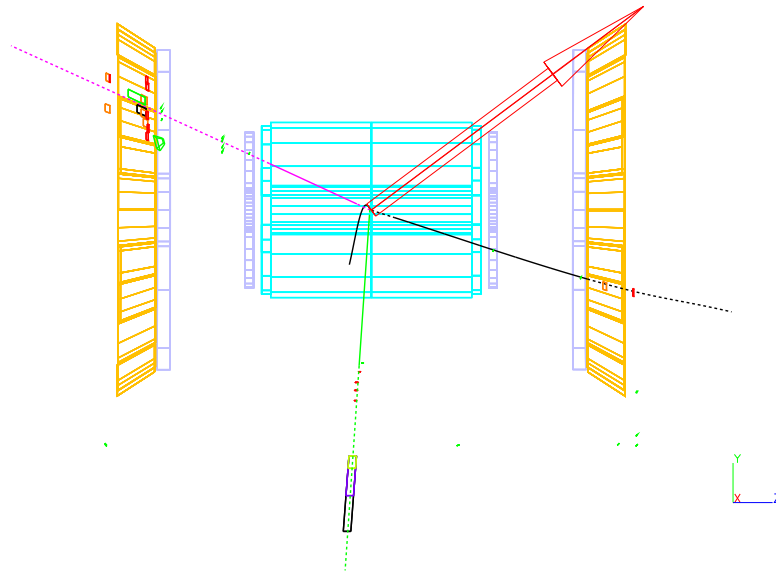



Figure 14: yz view of the first of the two neutralino pair production candidates decaying into four taus plus missing energy.

 DELPHI Beam: 91.6 GeV DAS: 26-Sep-1997 03:24:40	Run: 78409	Evt: 10676								
	Proc: 4-Dec-1997									
	Scan: 5-Mar-1998									
	Tan+DST									
				TD	TE	TS	TK	TV	ST	PA
Act	2	45	0	4	0	0	0	0	0	0
	(88) (101	X	0	I	4	I	0	I	0
Deact	0	0	0	0	0	0	0	0	0	0
	(0	X	0	X	0	X	4	I	0	I

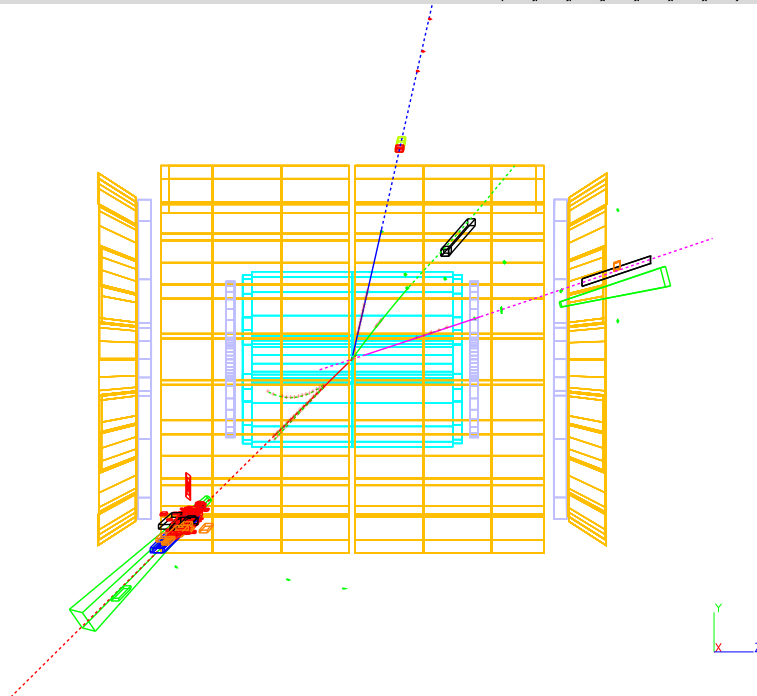


Figure 15: yz view of the second of the two neutralino pair production candidates decaying into four taus plus missing energy.

section for neutralino pairs was derived for each $m_{\tilde{\chi}_1^0}$, $m_{\tilde{\tau}_1}$ combination. A systematic error of 1.5% was assumed for the signal efficiency.

In what follows, the model described in reference [4] will be used in order to derive limits. This is a general model with the only assumptions of electroweak symmetry radiatively broken and null trilinear couplings at the messenger scale. The corresponding parameter space was scanned as follows: $1 \leq n \leq 4$, $5 \text{ TeV} \leq \Lambda \leq 900 \text{ TeV}$, $1.1 \leq M/\Lambda \leq 9000$, $1.1 \leq \tan \beta \leq 50$, and $\text{sign}(\mu) > 0$. n is the number of messenger generations in the model, Λ is the ratio between the vacuum expectation values of the auxiliary component superfield and the scalar component of the superfield and M is the messenger mass scale. $\tan \beta$ and μ are defined as for the MSSM.

Figure 16 shows the limit at the 95% C.L. on $\tilde{\chi}_1^0$ -pair production cross section, as a function of $m_{\tilde{\chi}_1^0}$ and $m_{\tilde{\tau}_1}$ after combining the results of the searches at $\sqrt{s} = 161, 172$ and 183 GeV with the maximum likelihood ratio method [28]. In this method, the ratios of the cross sections at different centre of mass energies, together with their respective collected luminosity, are used to weigh the results obtained at one energy against the others. For different n 's (the number of messenger generations), these ratios are bound to vary between certain limits. The same happens when considering scenarios with higgsino- or gaugino-like neutralinos. Figure 16 then presents the case for $n = 3$ and gaugino-like $\tilde{\chi}_1^0$. For the other scenarios considered in this study ($1 \leq n \leq 4$, and gaugino- or higgsino-like neutralinos), the maximum difference with respect to figure 16 occurs when $m_{\tilde{\chi}_1^0} < 80 \text{ GeV}/c^2$ and $m_{\tilde{\tau}_1} < 65 \text{ GeV}/c^2$, and is not bigger than 10%.

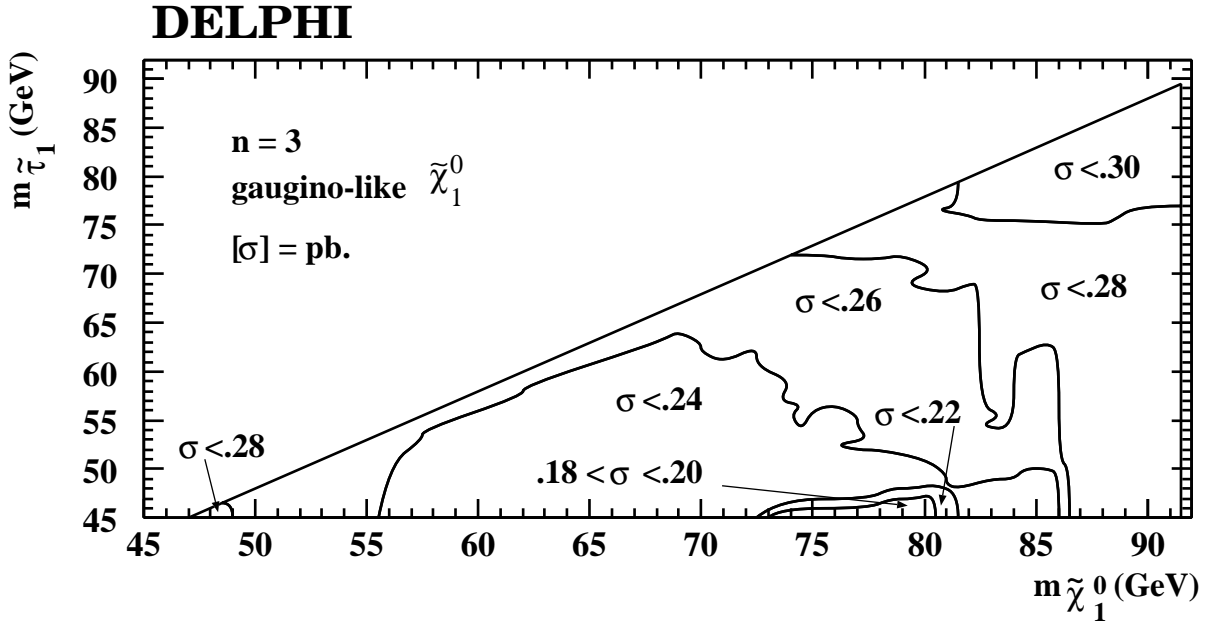


Figure 16: Limit at the 95% CL on $\tilde{\chi}_1^0$ -pair production cross section at $\sqrt{s} = 161, 172$ and 183 GeV , as a function of $m_{\tilde{\chi}_1^0}$ and $m_{\tilde{\tau}_1}$ for the case $n = 3$ and gaugino-like neutralinos, where n is the number of messenger generations.

Given the aforementioned limits on the production cross section, some sectors of the $(m_{\tilde{\tau}_1}, m_{\tilde{\chi}_1^0})$ space can be excluded. In order to achieve this for the largest area, two other analyses are taken into account. The first is the search for lightest neutralino pair production in the region of the parameter space where $\tilde{\chi}_1^0$ is the NLSP [11]. Within this

scenario, the neutralino decays into a gravitino and a photon. The second is the search for $\tilde{\tau}_1$ -pair production in the context of the MSSM. In the case where the MSSM $\tilde{\chi}_1^0$ is massless, the kinematics correspond to the case of $\tilde{\tau}_1$ decaying into a τ and a gravitino, except for spin effects, which are not taken into account in SUSYGEN.

Figure 17 shows the 95% C.L. excluded areas for the case $n = 2$ and gaugino-like neutralinos in the $m_{\tilde{\chi}_1^0}$ vs. $m_{\tilde{\tau}_1}$ plane. The positive-slope dashed area is excluded by this analysis. The resulting 95% C.L. lower limit on the mass of the lightest neutralino is $78 \text{ GeV}/c^2$. The negative-slope dashed area is excluded by the analysis searching for neutralino-pair production followed by the decay $\tilde{\chi}_1^0 \rightarrow \tilde{G}\gamma$. The cross hatched area is excluded by the direct search for MSSM $\tilde{\tau}_1$ -pair production [10], taking into account the possibility of $\tilde{\tau}_L - \tilde{\tau}_R$ mixing [7].

For other cases, lower limits for the mass of the lightest neutralino obtained with this analysis are described in table 5. In the case of $n = 1$ and gaugino-like lightest neutralino, the NLSP is always $\tilde{\chi}_1^0$, and the lower limit is derived from the search for acoplanar photons.

n	gaugino-like $\tilde{\chi}_1^0$ (GeV/c^2)	higgsino-like $\tilde{\chi}_1^0$ (GeV/c^2)
1	81.0	71.0
2	78.0	71.0
3	77.0	49.0
4	78.0	45.0

Table 5: Lower limits on $m_{\tilde{\chi}_1^0}$ for eight different scenarios. When $n = 1$ and the lightest neutralino is gaugino-like, the limit comes from the search for two acoplanar photons.

4.2 Stau pair production

No candidate was observed to pass the selection of the large impact parameter and secondary vertex searches while the total number of background events expected was 0.63 (0.37 on the vertex search and 0.26 on the large impact parameter search). The results of these analyses were combined with those of the stable heavy lepton search described in [9], which consider the $\tilde{\tau}_1$ decays outside the tracking devices ($R > 200 \text{ cm}$) and cover slepton masses from $45 \text{ GeV}/c^2$ up to the kinematic limit. Figure 9 shows the efficiency of the stable heavy lepton search (ε_3) for a stau mass of $60 \text{ GeV}/c^2$ at a centre of mass energy of 183 GeV as a function of the decay length. For very large $\tilde{\tau}_1$ masses, efficiencies around 80% were obtained by the heavy lepton search. Also shown is the combined efficiency of the three analyses (ε_{tot}), large impact parameter, vertex and heavy lepton analyses. As an event could be selected by the vertex search and by the stable heavy lepton search, the correlation was taken into account.

Upper limits at 95% CL on the production of $\tilde{\tau}_1$ were calculated for 183 GeV centre of mass energy. Figure 18 shows the cross section upper limit on the $m_{\tilde{G}}-m_{\tilde{\tau}_1}$ plane. The minimum upper limits achieved for a given $\tilde{\tau}_1$ were around 0.15-0.2 pb depending of $m_{\tilde{G}}$. For $m_{\tilde{G}} > 10 \text{ eV}/c^2$ and a $70 \text{ GeV}/c^2$ $\tilde{\tau}_1$, a 0.2 pb limit was obtained. One candidate was observed to pass the cuts of the small impact parameters search.

DELPHI

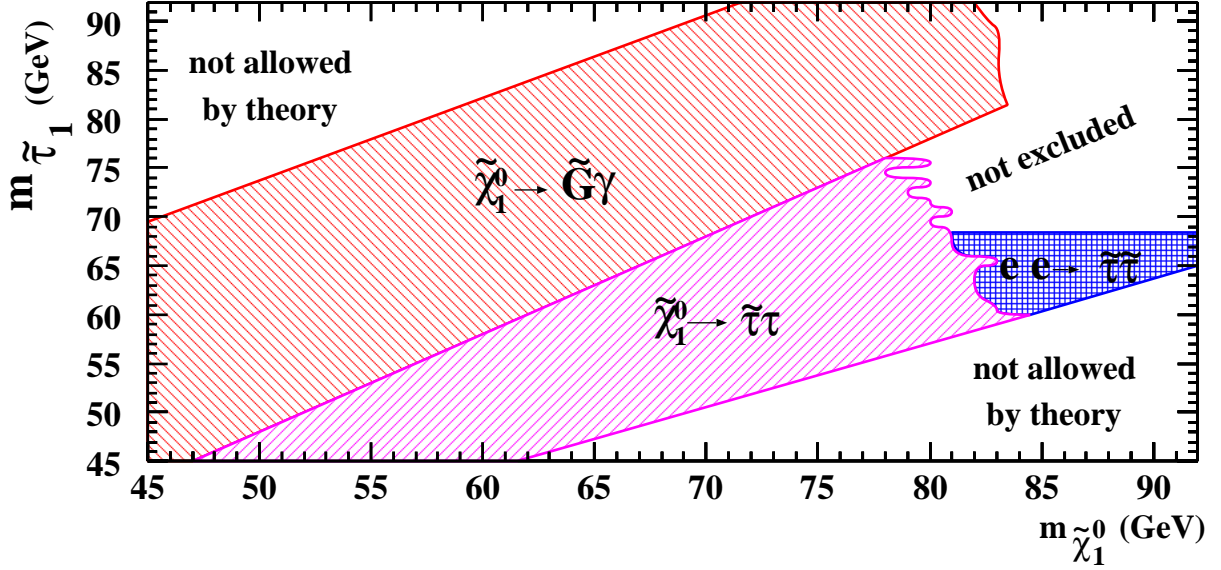


Figure 17: Areas excluded at the 95% CL for $n = 2$ and gaugino-like neutralinos in the $m_{\tilde{\chi}_1^0}$ vs. $m_{\tilde{\tau}_1}$ plane. The positive-slope dashed area is excluded by this analysis. The negative-slope dashed area is excluded by the search for $\tilde{\chi}_1^0 \rightarrow \gamma\tilde{G}$, and the cross hatched area by the direct search for MSSM stau-pair production.

The upper limits on the production cross section were used to exclude $m_{\tilde{\tau}_1}$ values as a function of $m_{\tilde{G}}$ combining all LEP2 energies, assuming conservatively the $\tilde{\tau}_1$ to be right-handed. The vertex analysis allows the exclusion $\tilde{\tau}_R$ masses between 70-77.5 GeV/ c^2 at 95% CL in the range of intermediate gravitino masses (25 to 150 eV/ c^2), the stable heavy lepton search covers the high gravitino mass region (over 100 eV/ c^2), while the impact parameter analysis covers the region of low gravitino masses.

Combining these results with the results of the search for MSSM $\tilde{\tau}_R$, allows the exclusion of stau masses below 68.5 GeV/ c^2 irrespective of the gravitino mass. The results are shown in Figure 19. Following ref [4] as in section 4.1, figure 20 shows the 95% C.L. excluded areas for the case of $n = 2$, gaugino-like neutralinos, and $m_{\tilde{G}} = 40$ eV/ c^2 in the $m_{\tilde{\chi}_1^0}$ vs. $m_{\tilde{\tau}_1}$ plane. The negative-slope dashed area is excluded by the analysis searching for neutralino-pair production followed by the decay $\tilde{\chi}_1^0 \rightarrow \tilde{G}\gamma$. The cross hatched area is excluded by this search, taking into account the possibility of $\tilde{\tau}_L - \tilde{\tau}_R$ mixing [7]. The resulting 95% C.L. lower limit on the mass of the lightest neutralino is 62 GeV/ c^2 , and that for the stau 60 GeV/ c^2 , from the neutralino-pair production search.

Figures 17 and 20 thus show that the search for neutralino pair production and stau pair production complement each other in different scenarios for the mass of the gravitino.

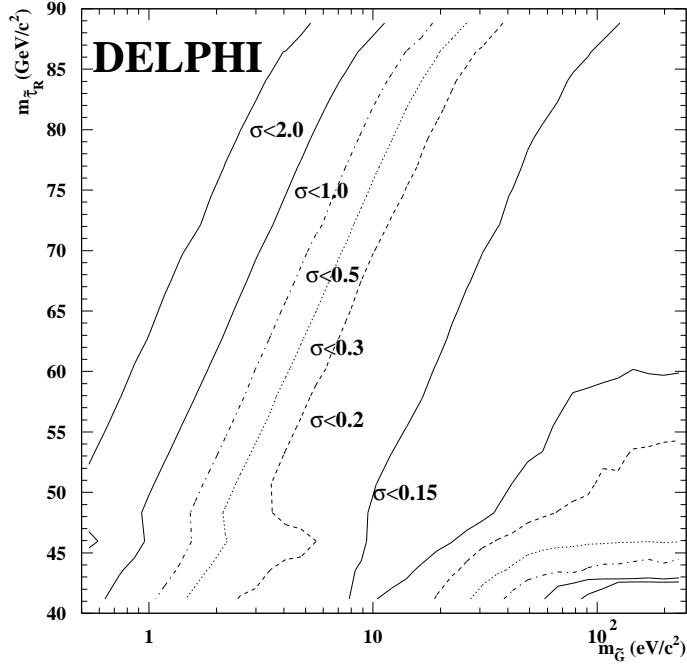


Figure 18: Upper cross section limit at 95% C.L. in the $(m_{\tilde{\tau}_1}, m_{\tilde{G}})$ plane for 183 GeV centre of mass energy obtained from the combination of the large impact parameter, vertex and heavy lepton searches.

5 Conclusions

Lightest neutralino and stau pair production were searched for in the context of light gravitino scenarios. Both searches were used in order to explore the $(m_{\tilde{\chi}_1^0}, m_{\tilde{\tau}_1})$ plane in different domains of the gravitino mass.

It was also shown that as the mass of the gravitino increases, there is less space covered by the search for neutralino pair production in the case of the lightest neutralino being the NLSP. A search for stau pair production, with stau decaying into a tau and a lightest neutralino, with the subsequent decay of the neutralino into a photon and a gravitino is foreseen for a future work.

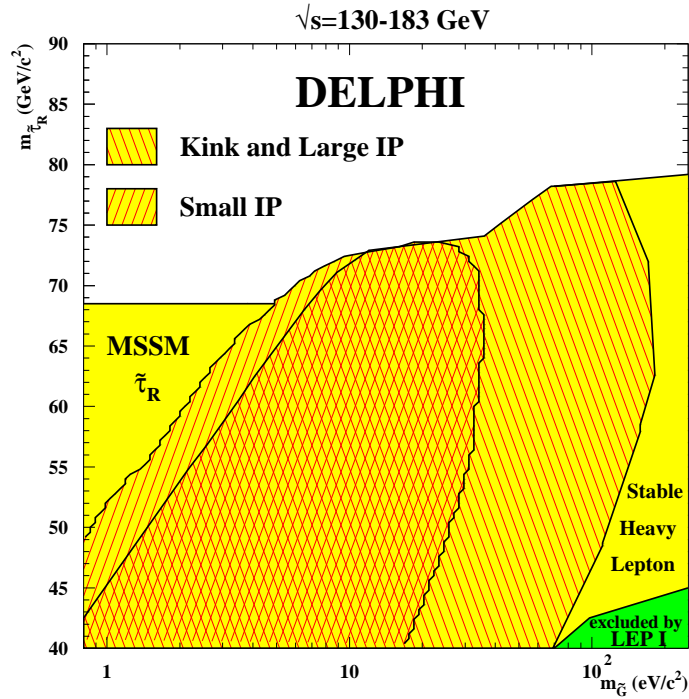


Figure 19: Exclusion region in the $(m_{\tilde{\tau}_R}, m_{\tilde{G}})$ plane at 95% CL for the present analysis combined with the stable heavy lepton search and the MSSM $\tilde{\tau}_R$ search, using all LEP-2 data. The positive slope hatched area shows the region excluded by the small impact parameter search. The negative slope hatched area shows the region excluded by the combination of the large impact parameter and kink searches.

References

- [1] M. Dine, W Fischler and M. Srednicki, Nucl. Phys. **B189** (1981) 575 ; S. Dimopoulos and S. Raby, Nucl. Phys. **B192** (1981) 353 ; M. Dine and W. Fischler, Phys. Lett. **B110** (1982) 227 ; M. Dine and M. Srednicki, Nucl. Phys. **B202** (1982) 238 ; L. Alvarez-Gaumé, M. Claudson and M. Wise, Nucl. Phys. **B207** (1982) 96 ; C. Nappi and B. Ovrut, Phys. Lett. **B113** (1982) 175 .
- [2] M. Dine and W. Fischler, Nucl. Phys. **B204** (1982) 346 ; S. Dimopoulos and S. Raby, Nucl. Phys. **B219** (1983) 479.
- [3] J. A. Bagger, K. Matchev, D. M. Pierce and R. Zhang, Phys. Rev. **D55** (1997) 3188.
- [4] D. A. Dicus, B. Dutta, S. Nandi, Phys. Rev. **D56** (1997) 5748 ; D. A. Dicus, B. Dutta, S. Nandi, Phys. Rev. Lett. **78** (1997) 3055.
- [5] F. Borzumati, hep-ph/9702307.
- [6] G.F. Giudice, R. Rattazzi, hep-ph/9801271, Submitted to Phys. Phys. Rev. D.
- [7] A. Bartl *et. al.*, Z. Phys. C73(1997) 469.

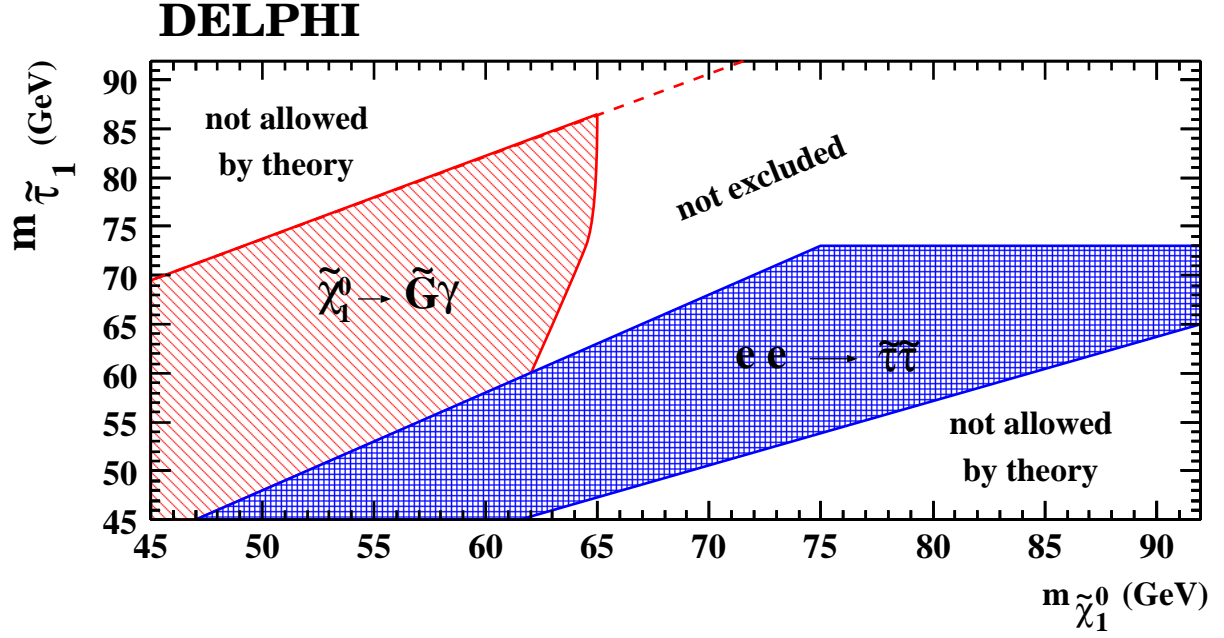


Figure 20: Areas excluded at the 95% CL for $n = 2$, gaugino-like neutralinos, and $40 \text{ eV}/c^2$ gravitinos, in the $m_{\tilde{\chi}_1^0}$ vs. $m_{\tilde{\tau}_1}$ plane. The negative-slope dashed area is excluded by the search for $\tilde{\chi}_1^0 \rightarrow \gamma\tilde{G}$, and the cross hatched area by this analysis.

- [8] S. Dimopoulos, M Dine, S Raby, S. Thomas and J. D. Wells, Nucl. Phys. Proc. Suppl. **52A** (1997) 38.
- [9] P. Abreu et al., Phys. Lett. **B396** (1997) 315 and contribution to ICHEP'98.
- [10] Contribution to ICHEP'98
- [11] DELPHI Note 98-7 PHYS 758. See the last one when it gets a number.
- [12] P. Abreu et al, PPE paper 189. To be submitted to E. Phys. J. C.
- [13] P. Aarnio et al., Nucl. Instr. and Meth. **303** (1991) 233.
- [14] P. Abreu et al., Nucl. Instr. and Meth. **378** (1996) 57.
- [15] T. Sjöstrand, Comp. Phys. Comm. **39** (1986) 347;
T. Sjöstrand, PYTHIA 5.6 and JETSET 7.3, CERN-TH/6488-92.
- [16] DELPHI Coll., P. Abreu *et al.*, Z. Phys. **C73** (1996) 11.
- [17] SUSYGEN 2.12, S. Katsanevas and S. Melachroinos in *Physics at LEP2*, CERN 96-01, Vol. 2, p. 328 and <http://lyohp5.in2p3.fr/delphi/katsan/susygen.html> .
- [18] J.E. Campagne and R. Zitoun, Z. Phys. **C43** (1989) 469.
- [19] S. Jadach and Z. Was, Comp. Phys. Comm. **79** (1994) 503.
- [20] F.A. Berends, R. Kleiss, W. Hollik, Nucl. Phys. **B304** (1988) 712.

- [21] F.A. Berends, R. Pittau, R. Kleiss, *Comp. Phys. Comm.* **85** (1995) 437.
- [22] S. Nova, A. Olshevski, and T. Todorov, *A Monte Carlo event generator for two photon physics*, DELPHI note 90-35 (1990).
- [23] F.A. Berends, P.H. Daverveldt, R. Kleiss, *Comp. Phys. Comm.* **40** (1986) 271, *Comp. Phys. Comm.* **40** (1986) 285, *Comp. Phys. Comm.* **40** (1986) 309.
- [24] DELPHI Collaboration, P. Abreu *et al.*, *E. Phys. J. C1* (1998)1.
- [25] S. Catani, *Phys. Lett.* **B269** (1991) 432 .
- [26] P. Abreu *et al.*, Search for Neutr Heavy Leptons produced in Z decays. *Zeit. Phys.* C74 (1997) 57.
- [27] P. Billoir and S. Qian, *Nucl. Instr. and Meth.* **311** (1992) 139.
- [28] A.L. Read, DELPHI 97-158 PHYS 737 and references therein.